energies

MDPI

Article

Optimal Capacity of a Battery Energy Storage System Based on Solar Variability Index to Smooth out Power Fluctuations in PV-Diesel Microgrids

Julius Susanto [1,2] and Farhad Shahnia [2,*]

[1] Australian Energy Market Commission (AEMC), Perth 6000, Australia; julius.susanto@murdoch.edu.au
[2] School of Engineering and Energy, Murdoch University, Perth 6150, Australia
* Correspondence: f.shahnia@murdoch.edu.au

Abstract: Battery energy storage systems can be integrated with photovoltaic (PV)-diesel microgrids as an enabling technology to increase the penetration of PV systems and aid microgrid stability by smoothing out the power fluctuations of the PV systems. This paper focuses on this topic and aims to derive correlations between the optimal capacity of the smoothing batteries and variabilities in the daily solar irradiance. To this end, the two most commonly used moving average and ramp rate control techniques are employed on a real solar irradiance dataset with a 1-min resolution for a full calendar year across 11 sites in Australia. The paper then presents the developed empirical model, based on linear regressions, to estimate the batteries' optimal capacity without requiring detailed simulation studies, which are useful for practitioners at the early stages of a project's feasibility evaluation. The performance of the developed technique is validated through numerical simulation studies in MATLAB®. The study demonstrates that the empirical model provided reasonably accurate estimates when using the moving average smoothing technique but had limited accuracy under the ramp rate control technique.

Keywords: PV-diesel microgrid; power smoothing battery; solar irradiance variability

Citation: Susanto, J.; Shahnia, F. Optimal Capacity of a Battery Energy Storage System Based on Solar Variability Index to Smooth out Power Fluctuations in PV-Diesel Microgrids. *Energies* **2023**, *16*, 5658. https://doi.org/10.3390/en16155658

Academic Editors: Ignacio Hernando-Gil and Ionel Vechiu

Received: 11 July 2023
Revised: 20 July 2023
Accepted: 25 July 2023
Published: 27 July 2023

1. Introduction

There are thousands of standalone remote area power systems and microgrids around the world that supply remote and island communities that do not have access to the grid. Most of these systems rely solely on diesel generators [1]. However, diesel generators are expensive, and in recent years, with the rapid decline in the costs of photovoltaic (PV) systems, PV systems have become significantly more competitive than diesel on a levelized cost of energy basis [2]. There is, therefore, growing interest in hybridizing diesel-based microgrids with PV systems and maximizing the penetration of the PV component (see Figure 1).

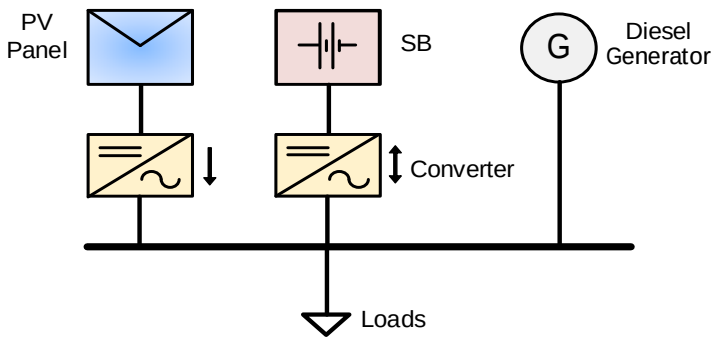

Figure 1. A typical PV-diesel microgrid with a power smoothing battery (SB).

However, there are technical limits to the penetration of PV systems into a diesel microgrid, which are associated with factors such as the frequency stability and underloading of the diesel generators [3]. One option to increase the penetration of PV systems is to use enabling technologies, such as battery energy storage systems, to smooth out the fluctuations in the output power of PV systems [4–6], thereby limiting frequency deviations and reducing the wear and tear on the diesel generators from excessive ramping [7]. Energy storage systems are commonly used for integrating renewable energy resources into microgrids [8,9], and there have recently been significant developments in their chemical aspects and capacities [10–12].

Traditionally, the sizing of battery energy storage systems for smoothing the power fluctuations of PV systems has been achieved through chronological/time-sequential simulation studies, where a smoothing algorithm is applied to the PV system's output and the energy exchange between the battery and the power system is calculated at each time step [13–22]. Similar methods are also used to smooth wind power fluctuations [23–28]. For the smoothing of PV fluctuations, the application of high-resolution solar irradiance data (i.e., less than 1 min) is necessary to adequately reflect the extent of short-term variability in the solar irradiance [29]. However, several previous studies have used coarse 1-h resolution data, which would introduce significant temporal smoothing from the solar irradiance data alone [16,19]. Moreover, data for at least a year should be used for sizing a smoothing battery (SB) to capture the seasonal variations in the solar irradiance variability [14,16]. Some studies, such as [13,20], have only considered data for one day, while [21] examined only 1 h of data. Finally, while some studies, such as [16,17,21], make use of fully specified battery capacity models, many researchers have not considered the battery charge/discharge characteristics and they have sized the battery capacity based on either the peak energy exchange [18,19] or the net energy exchange [20].

Furthermore, in some studies, there is also no consideration for key parameters such as the battery's depth of discharge (DoD) and the initial state of charge (SoC) [21,23]. It should be noted, however, that many of these previous works are predominantly concerned with the control and performance aspects of different smoothing algorithms, and battery sizing is not their main emphasis. Table 1 summarizes the key features of the studies mentioned above (i.e., using low/high resolution and the considered period of solar irradiance data, considering various geographic locations, and employing a detailed battery model).

Table 1. The key features in the existing literature on sizing of SBs.

Refs.	High-Resolution Data	≥1 Year of Solar Data	Multiple Locations	Battery Model
[7,13]	✓ (20 s)	✗ (1 day)	✗	✗
[14,15]	✓ (5 s)	✓ (1 year)	✗	✗
[16]	✗ (1 h)	✓ (1 year)	✓ (two)	✓ (Kinetic)
[17]	✗ (1 h)	✓ (1 year)	✓ (two)	✓ (Kinetic)
[18]	✓ (1 min)	✗ (1 day)	✗	✗
[19]	✗ (1 h)	✗ (1 day)	✗	✗
[20]	✓ (30 s)	✗ (1 day)	✗	✗
[21]	✓ (≤1 min)	✗ (1 h)	✗	✓ (Internal resistance)
This paper	✓ (1 min)	✓ (1 year)	✓ (11)	✓ (Kinetic)

Against this backdrop, this paper aims to address some of the shortcomings of previous works by developing a comprehensive methodology for the optimal sizing of SBs employed in PV-diesel microgrids, using one year of high-resolution solar irradiance data across multiple geographically diverse sites and using a fully specified battery capacity model.

Furthermore, this paper investigates the correlations between the SB's optimal capacity (SBOC) and the solar irradiance variability index (SIVI) and proposes an empirically derived estimate for the optimal battery size that can be calculated without simulation studies. Table 1 also shows the key features of the proposed technique in this paper.

In summary, the main contributions of this work are:

- Proposing to consider the impact of the SIVI in determining the SBOC in PV-diesel microgrids and determining their correlation;
- Developing empirical estimates, based on linear regressions, to estimate the SBOC by only considering the SIVI and without requiring the use of detailed simulation studies;
- Defining the sensitivity of the SBOC versus the battery and ambient parameters.

The remainder of the paper is organized as follows: Section 2 discusses how solar irradiance fluctuations throughout a day can be measured and quantified with the SIVI. The considered PV-diesel microgrid with the proposed SB is introduced in Section 3; this section also discusses the proposed approaches to determining the SBOC. The relationships between the SBOC and the SIVI are derived in Section 4 through numerical analyses over a real dataset from 11 weather stations around Australia. The performance of the proposed technique versus two existing approaches in the literature are presented in Section 5. Section 6 discusses the sensitivity of the SBOC against the key system design parameters, while the practical considerations and limitations of the SBOC determination are briefly discussed in Section 7. Finally, the key findings of the research are summarized and highlighted in Section 8, while two appendices provide details of the employed modeling approach and technical parameters in the studies of this paper.

2. Solar Irradiance Variability

One of the key features of this paper is the explicit consideration of the SIVI for sizing an SB. This is because various geographical locations are subject to different levels of the SIVI over a calendar year and, consequently, the sites with a low SIVI do not require as much smoothing as the sites with a higher SIVI.

The solar irradiance dataset used in this study is based on the 2017 measurement data of the global horizontal irradiance (GHI), with a 1-min resolution, captured from the Australian Government's Bureau of Meteorology [30]. These data were retrieved for 11 weather station locations around Australia, as listed in Table 2. The selected areas vary from urban (site-1, 6) to rural (site-4, 8) locations, coastal (site-7, 8, 9) to inland areas (site-2, 5), and hot (site-3, 11) to cold (site-4, 10) regions.

Table 2. Considered study sites in this study.

Site	Name	State	Longitude (°)	Latitude (°)
1	Adelaide	South Australia	−34.9285	138.6007
2	Alice Springs	Northern Territory	−23.6980	133.8807
3	Rockhampton	Queensland	−23.3791	150.5100
4	Cape Grim	Tasmania	−40.6833	144.6833
5	Kalgoorlie	Western Australia	−30.7490	121.4660
6	Darwin	Northern Territory	−12.4634	130.8456
7	Broome	Western Australia	−17.9614	122.2359
8	Learmonth	Western Australia	−22.2312	114.0888
9	Geraldton	Western Australia	−28.7774	114.6150
10	Wagga	New South Wales	−35.1082	147.3598
11	Townsville	Queensland	−19.2590	146.8169

Fluctuations of the solar irradiance throughout a full day at a specific location can be quantified as a single number using the SIVI in the form of [31]:

$$SIVI = \frac{\sum_{t=1}^{T-1} \sqrt{[GHI(t+1) - GHI(t)]^2 + \Delta T^2}}{\sum_{t=1}^{T-1} \sqrt{\left[GHI_{\text{clear-sky}}(t+1) - GHI_{\text{clear-sky}}(t)\right]^2 + \Delta T^2}} \quad (1)$$

where GHI is the measured global horizontal irradiance (W/m^2), $GHI_{\text{clear-sky}}$ is the clear-sky irradiance, and ΔT is the averaging interval, while T is the number of consecutive measurements (e.g., given a minute-averaged time series, $\Delta T = 1$ and $T = 1440$ for a 24-h period).

The SIVI provides a useful measure for classifying different days based on their solar intermittency relative to the expected clear-sky irradiance profile. A SIVI of close to unity represents the ideal clear-sky day (refer to Figure 2a, as an example, captured from site-1 on 25 January 2017), while a high SIVI is more representative of a mixed-sky day (refer to Figure 2b, captured from the same site on 6 November 2017). Note that an overcast day may have a low SIVI despite having uniformly low irradiance throughout the day (as an example, see Figure 2d, captured from the same site on 16 July 2017).

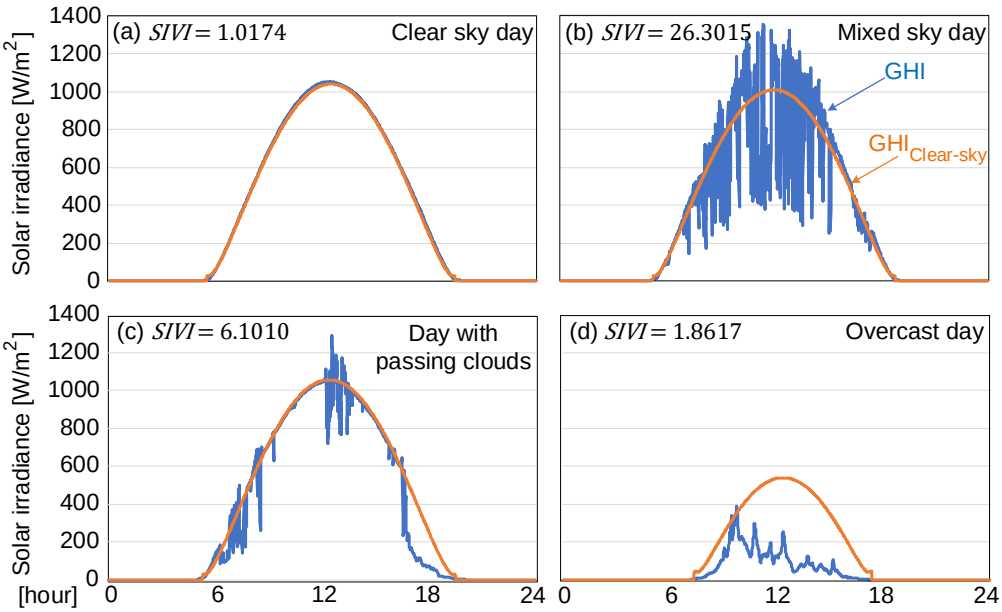

Figure 2. Solar irradiance and the corresponding $SIVI$ for 4 sample days at site-1: (**a**) a clear sky day, (**b**) a day with frequent cloud movements, (**c**) a clear day with a few passing clouds throughout the day and an overcast period in the afternoon, (**d**) an overcast day.

The SIVI for a single location can be calculated for each day in the available dataset, with a minimum of one year to cover seasonal variations and combined to form empirical non-parametric cumulative distribution functions (CDFs), instead of the true CDF. The CDFs provide insights into a site's SIVI over time.

Figure 3 illustrates the empirical CDFs for sites-1 to -4 in Table 2 in 2017. As seen in Figure 3b, site-2 shows SIVIs close to unity for over 40% of the year, indicating a site with consistent clear sky days. On the other hand, as seen in Figure 3c, site-3 exhibits a much higher spread in the SIVI, suggesting a site with a higher prevalence of mixed-sky days.

The SIVI data in the CDFs can also be represented as a probability of non-exceedance (PONE) values, which indicate the probability that a SIVI is not exceeded. For example, Table 3 provides the SIVI values under various PONE limits for the four sites of Figure 3. As seen from this table, at site-2, a P90 value of 10.2 denotes that the SIVI does not exceed

10.2 for 90% of the year. The PONE limits will be used in the remainder of the paper to select an appropriate smoothing level for the SBs at various locations.

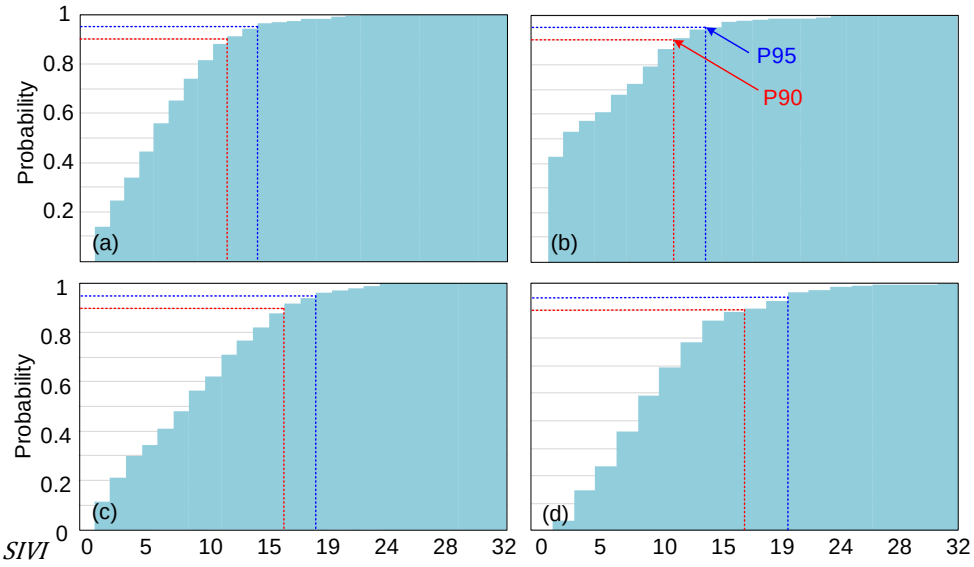

Figure 3. Empirical CDF for $SIVI$ in 2017 at (**a**) site-1, (**b**) site-2, (**c**) site-3, (**d**) site-4.

Table 3. SIVIs for various PONE levels for sites-1 to -4 in Table 2 in 2017.

PONE	Site-1	Site-2	Site-3	Site-4
P50	4.8	2.0	8.4	8.2
P75	7.2	8.4	12.5	12.1
P90	11.1	10.2	15.3	15.4
P95	12.4	12.7	17.8	18.5
P99	22.1	21.3	22.5	23.4
P100	26.3	25.0	25.0	32.9

3. Simulation Model and Determination of SB Capacity

The system topology considered in this article is an ac-coupled PV-diesel microgrid supplying ac loads, as shown in Figure 1. The SB's functionality in such systems is to smooth out the fluctuations in the output power of the PV systems in order to limit the ramping requirements and stresses on the diesel generator(s). This is crucial for increasing the PV penetration in the microgrid without causing frequency instability and poor frequency regulation.

For this study, neither the diesel generator nor the loads are explicitly modelled as the study specifically looks at the SB's performance in producing a less volatile output from the solar PV system. It is assumed from the design of the microgrid that the diesel generator and PV system have been adequately sized to supply the load at all times without under- or over-loading the diesel generator. Based on the diesel generator specifications, the maximum ramp-rate capability of the generator defines the amount of smoothing required by the SB [32].

3.1. Power Smoothing Algorithms

Several methods exist in the literature regarding power smoothing algorithms via batteries [14,15,33,34], among which two commonly used techniques are considered here, as discussed below:

3.1.1. Moving Average (MA) Technique

The lagging MA-based smoothing technique takes the arithmetic mean of the PV system's output power for the previous N_w time steps from the current time step of t as [33,34]:

$$P_{\mathrm{MA}}(t) = \frac{\sum_{i=0}^{N_w-1} P_{\mathrm{PV}}(t-i)}{N_w} \tag{2}$$

where $P_{\mathrm{MA}}(t)$ is the smoothed PV power output at time step t [W], $P_{\mathrm{PV}}(t)$ is the raw PV power output at that time step [W], and N_{w} is the window of the MA, measured as the integer number of time steps.

3.1.2. Ramp Rate Control (RR) Technique

The RR-based smoothing technique limits the change in the output power between 1-min time steps to a maximum value. In this study, the maximum allowable change in the output power is expressed as a proportion relative to the nominal output power of the PV system, in the form of:

$$\Delta P_{\max} = k_{\mathrm{RRL}} \times P_{\mathrm{nom}} \tag{3}$$

where $\Delta P_{\max}$ is the maximum allowed change in the PV power output [W], k_{RRL} is the ramp rate limit [%], and P_{nom} is the nominal output of the PV module at standard test conditions in watt peak [Wp]. The target output power by this technique ($P_{\mathrm{RR}}(t)$) is then:

$$P_{\mathrm{RR}}(t) = \begin{cases} P_{\mathrm{PV}}(t-1) - \Delta P_{\max} & \text{if} \quad |\Delta P_{\mathrm{PV}}| > \Delta P_{\max} \;\&\; \Delta P_{\mathrm{PV}} < 0 \\ P_{\mathrm{PV}}(t) & \text{if} \quad |\Delta P_{\mathrm{PV}}| \le \Delta P_{\max} \\ P_{\mathrm{PV}}(t-1) + \Delta P_{\max} & \text{if} \quad |\Delta P_{\mathrm{PV}}| > \Delta P_{\max} \;\&\; \Delta P_{\mathrm{PV}} > 0 \end{cases} \tag{4}$$

where $\Delta P_{\mathrm{PV}} = P_{\mathrm{PV}}(t) - P_{\mathrm{PV}}(t-1)$ is the change in the output power of the PV system between time steps t and $t-1$.

At each time step, the SB's net output power ($P_{\mathrm{SB}}^{\mathrm{MA}}(t)$) is the difference between the SB's target output power and the PV's output power at that time step, i.e.,

$$P_{\mathrm{SB}}^{\mathrm{MA}}(t) = P_{\mathrm{MA}}(t) - P_{\mathrm{PV}}(t) \tag{5}$$

$$P_{\mathrm{SB}}^{\mathrm{RR}}(t) = P_{\mathrm{RR}}(t)min - P_{\mathrm{PV}}(t) \tag{6}$$

for the MA- and RR-based techniques, respectively. By convention, a positive power (i.e., $P_{\mathrm{SB}}(t) > 0$) denotes the SB discharges, while a negative power denotes the SB's charging.

3.2. SB's Capacity

The SBOC can be determined in the form of a problem that aims to find the SB's best (smallest) nominal energy storage capacity ($E_{\mathrm{SB}}^{\mathrm{nom}}$) as:

$$SBOC = \min E_{\mathrm{SB}}^{\mathrm{nom}} \tag{7}$$

which is subject to $SoC_{\min} < SoC(t) \le SoC_{\max}$, while $SoC_{\min}$ and $SoC_{\max,}$ respectively, denote the SB's minimum and maximum allowed SoC. $E_{\mathrm{SB}}^{\mathrm{nom}}$ is the nominal capacity of the SB (in kWh), i.e., the maximum amount of energy that the SB can store fully charged. Note that $E_{\mathrm{SB}}^{\mathrm{nom}}$ is simply a decision variable to be determined; i.e., it is an assumed input value (not calculated).

One approach to solving (7) is to iteratively run chronological simulations in order to find the smallest $E_{\mathrm{SB}}^{\mathrm{nom}}$ that satisfies the SoC constraints. This approach is hereafter referred to as the 'chronological simulation method', as discussed in Appendix A.

3.3. Proposed Approximate Method Based on SIVI

Although the chronological simulation method is more accurate, it is computationally intensive and not necessarily amenable to practical scenarios, especially when conducting

preliminary-level project feasibility and screening studies. As such, an approximate method is proposed in this paper that has an order-of-magnitude accuracy but leads to very fast results.

This technique is derived by applying the chronological simulation method for each day (refer to Appendix A) and across all sites in Table 2, and then performing a linear regression on the combined results with the SIVI as the dependent variable. A statistical error term (i.e., the standard error) is also added to the regression to capture the upper envelope of the results. The approximated SBOC based on the linear regression (denoted by $SBOC^{ap}$) is calculated as:

$$SBOC^{ap} = \alpha \times SIVI + \beta + \sigma \tag{8}$$

where α and β are the linear regression coefficients and σ is the standard error of the estimate, which is calculated from:

$$\sigma = \sqrt{\frac{\sum\left(E_{SB}^{nom} - \left(E_{SB}^{nom}\right)^{pred}\right)^2}{N_s}} \tag{9}$$

where E_{SB}^{max} is the SBOC for a single day, while $\left(E_{SB}^{max}\right)^{pred} = \alpha \times VI + \beta$ is the SB's capacity predicted by the linear regression, and N_s is the total number of samples.

The SIVI can be estimated based on the site location or nearby sites with complete measurement data. If daily SIVI data are available, then a smoothing level (e.g., P90 or P95) can be selected, as described in Section 2. For example, if the P90 SIVI is 22 and given the coefficients of $\alpha = 0.0046$, $\beta = 0.0567$, and $\sigma = 0.0315$ (applicable for the MA technique with a 10-min window), the approximate SBOC calculated from (8) will be 0.1894 kWh/kWp, i.e., a SB with $E_{SB}^{nom} = 0.1894$ kWh is needed for every one kWp of the PV system.

4. Performance Evaluation

Let us consider the microgrid in Figure 1 with a standard crystalline silicon PV array connected via a grid-tied inverter. Also, a deep-cycle valve-regulated lead-acid SB is considered in the system. The modeling of the PV system and SB are discussed in Appendix B, while the employed model parameters for the PV system are provided in Table A1 in Appendix C. The SB's assumed discharge characteristics are based on an Olympic Batteries DC2-500 type battery [35], as listed in Table A2 in Appendix C. The battery's model is assumed to be the Kinetic model and the same as the models employed in similar works such as [16,17]. The bi-directional converter for the SB is considered to have an efficiency of 94%, based on the data from a Tier-1 manufacturer [36]. For the base case studies, the SB's DoD is assumed as 70% and the SB is configured at the beginning of each day with an initial SoC of 80%. It is to be noted that although considering different battery and converter characteristics will modify the output numerical results of the study, it will not impact the successful performance of the proposed approximate method for determining the SBOC based on the SIVI. The ambient temperature data are retrieved from the Bureau of Meteorology; however, only historical daytime maximum temperatures for each day were accessible in the public dataset. Therefore, the ambient temperature is assumed to be constant throughout the day and set as the historical maximum temperature in the studies. This is a conservative assumption and leads to a higher temperature derating of the PV system's output power. It is noteworthy that when the study was repeated whilst considering hourly ambient temperature data (based on straight line intra-hour interpolation) instead of a constant ambient temperature for the whole day, the determined SBOC did have a marginal difference. This is mainly because the SBOC is primarily driven by fluctuations in the output power of the PV systems over a typical timescale of 5 to 20 min and relative changes in the average ambient temperature over such timescales are not very large.

4.1. Single-Day Study Results

The simulation model is run for a 24-h period for site-1 on 5 February 2017 to illustrate the effects of the MA- and RR-based techniques on the SB's output power and the final smoothed output from the combined PV-battery system. The considered day is a mixed-sky day with a moderately high *SIVI* of 20.91. For the single day simulations, an unoptimized SB capacity of 1 kWh is applied in order to facilitate comparisons of the SB's performance between the simulation results. Note that the selection of an SB of 1 kWh is arbitrary and is only used for demonstrating an example of the time-series plots of the smoothing methods and the effect of the different parameters on both the smoothing performance and battery usage. The results of the study are demonstrated in Figures 4 and 5, respectively, for the MA- and RR-based techniques. For each technique, the study was conducted with two different smoothing parameters (i.e., MA window and RR limit) to demonstrate the impact of more onerous smoothing requirements. As can be seen from these figures, a larger MA window (20 vs. 5 min) or a tighter RR limit (1 vs. 10%) produces a smoother output, but a larger proportion of the battery capacity is used as a result.

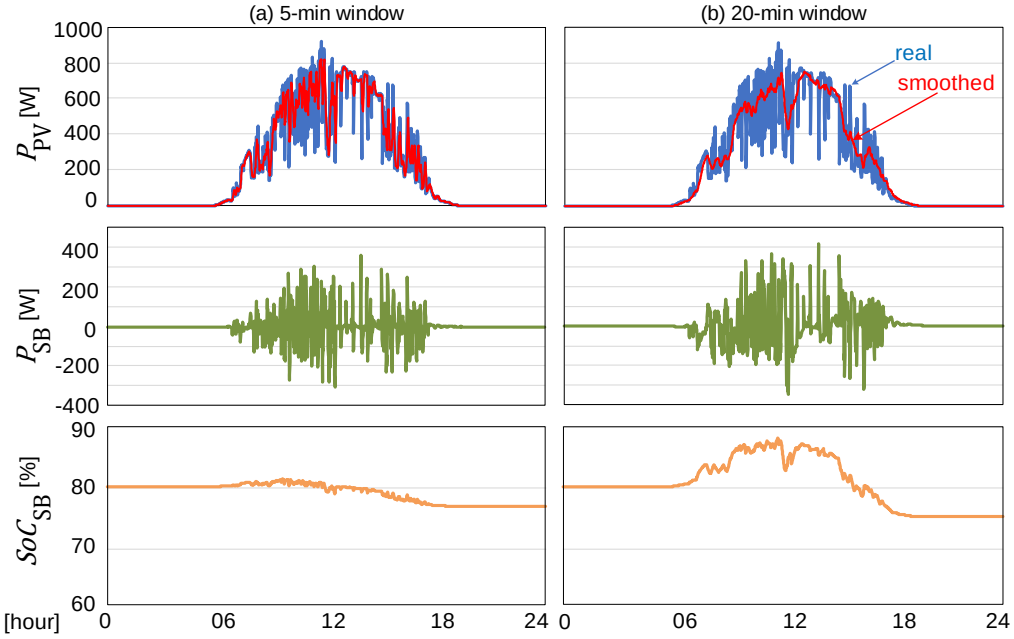

Figure 4. Performance of the microgrid in Figure 1 when using an SB, defined under the MA technique for a single day (15 February 2017 at site-1) with a window of (**a**) 5, (**b**) 20 min.

4.2. SB Selection Results

The chronological simulation method in Appendix A was applied to the 11 sites in Table 2 for each day over the full calendar year of 2017. Figure 6a,b illustrate the results for four sites when the MA and RR techniques were employed. The study attempts to determine the minimum SBOC required to meet the selected smoothing criteria for a given day and site. For each site, the results are presented as a scatter plot, where each point represents the SB's optimized capacity for a single day (on the *y*-axis) and the corresponding SIVI for that day (on the *x*-axis). An empirical CDF of the optimized SB capacities over the full year is also shown to illustrate how the results are distributed and aid in the SBOC's selection.

The results are expressed as the kWh of the SB's capacity per kWp of the PV systems and can be scaled linearly to any desired PV capacity. As such, if the study yields an SBOC of 0.4 kWh per kWp, then a 100 kWp PV system would require an SB with a capacity of 40 kWh.

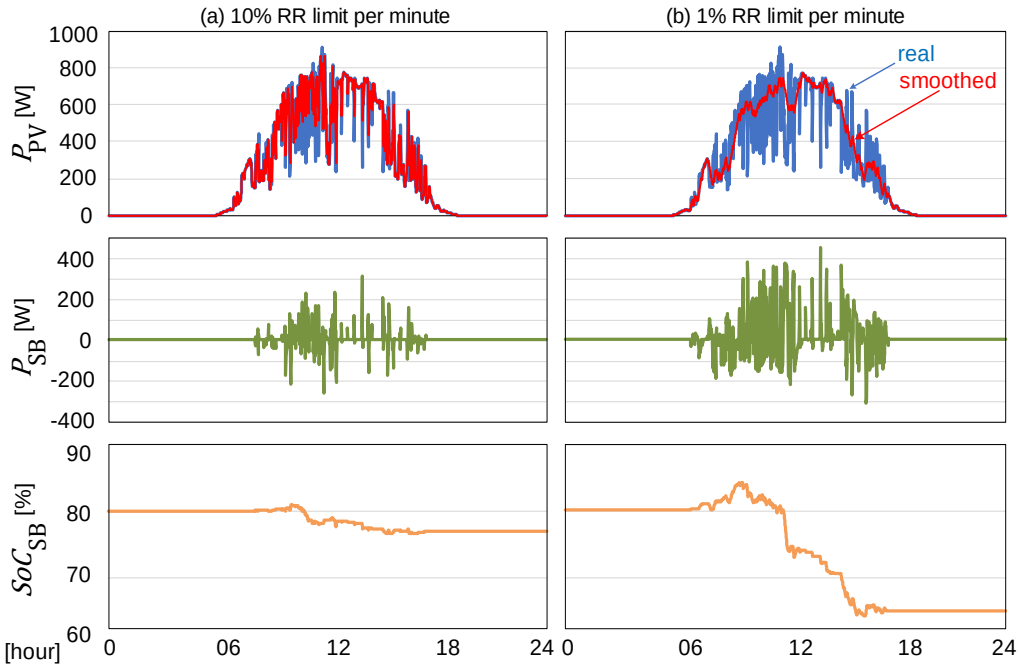

Figure 5. Performance of the microgrid in Figure 1 when using an SB, defined under the MA technique for a single day (15 February 2017 at site-1) assuming a window of (**a**) 10%, (**b**) 1%.

The results for the MA-based technique in Figure 6a illustrates a clear positive correlation between the SBOC and the SIVI. This result is according to the general expectation of observing higher levels of the SB's charge/discharge during days with a high SIVI and vice versa. However, the results for the RR-based technique in Figure 6b demonstrate a weaker correlation between the SBOC and the SIVI. Indeed, a comparison of the Pearson correlation coefficients between the SBOC using the MA and RR techniques with the observed SIVI in Table 4 indicates that, across all of the studied sites, the RR-based technique is less strongly correlated than the MA-based technique (e.g., the average correlation coefficient across all sites is 0.7862 when using the MA technique versus 0.5556 when using the RR technique).

Comparing the empirical CDFs for the MA and RR techniques given in Figure 6a,b indicates that while the SBOC determined by the MA technique appears symmetrically distributed, the RR is positively skewed, with the mode centered around zero. This makes intuitive sense because with the RR, there are clear-sky days for more than 80% of the studied time (i.e., SIVI close to 1) where no smoothing is required; thus, a smaller SBOC is needed. On the other hand, the diurnal nature of the sun results in the MA algorithm requiring energy exchange with the SB, even during clear-sky days (provided that the MA window is sufficiently large) [34]. This is in line with the finding of [14], which shows increased SB cycling and degradation under the MA technique relative to the RR technique.

To understand why the RR is less strongly correlated with the SIVI, let us consider the single-day simulations at site-5 for two different days—20 November 2017 and 18 December 2017—illustrated, respectively, in Figure 7a,b. On the first day, the SIVI is 10.43, and Figure 7a shows a mainly clear-sky day with rapidly moving cloud bands occurring in the middle of the day and afternoon. In contrast, the SIVI on the second day is 23.04, and Figure 7b shows a highly variable mixed-sky day with solar irradiance fluctuations occurring consistently throughout the day. However, the SBOC for the relatively low SIVI on the mainly clear-sky day in Figure 7a is 0.2837 kWh/kWp, while it is almost ten-times lower (0.029 kWh/kWp) for the high SIVI on the mixed-sky day in Figure 7b, which is contrary to what is expected.

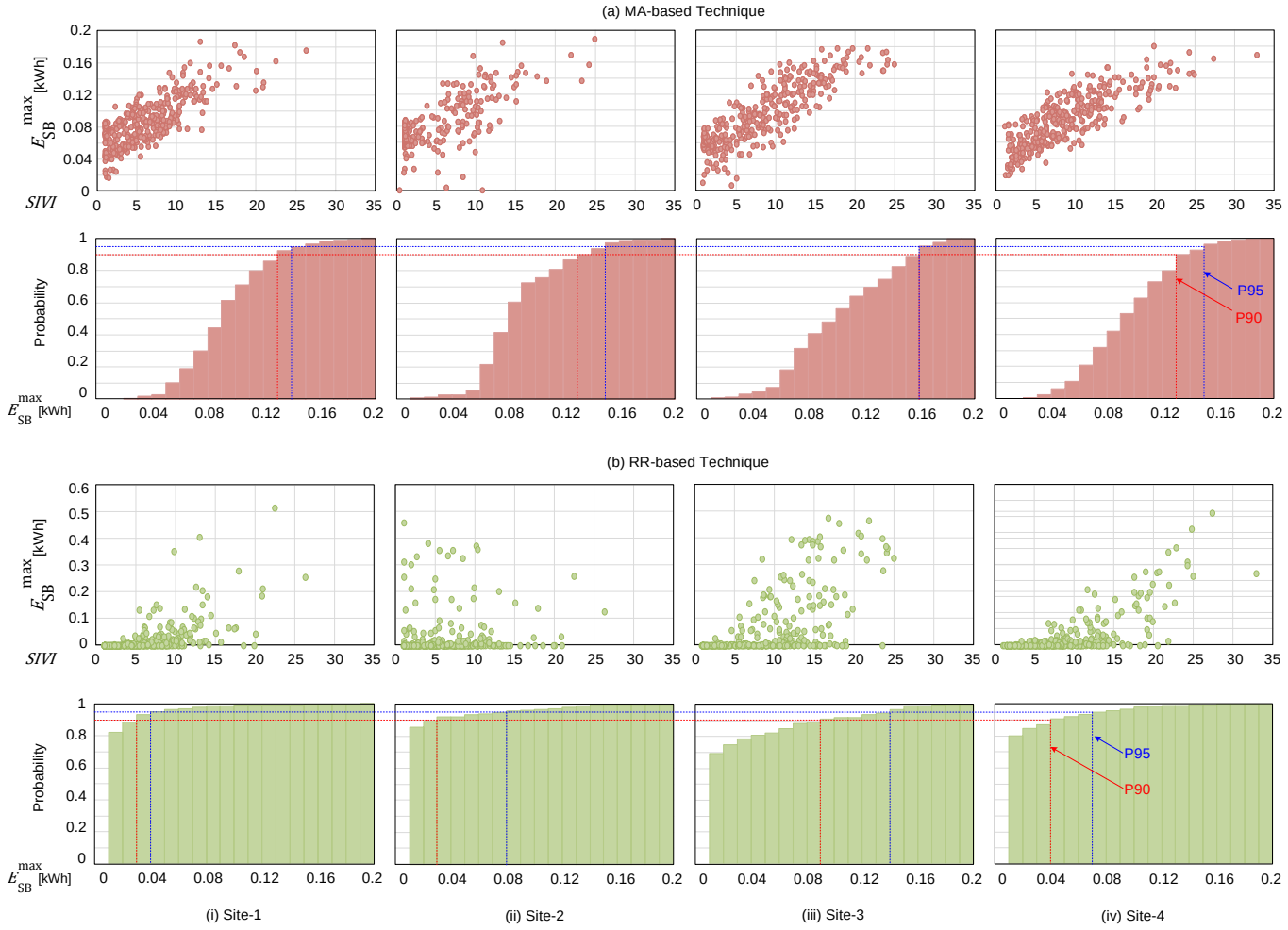

Figure 6. The SB's selection results (scatter plot of the SBOC versus $SIVI$ and their CDF) using the detailed model with P90 or P95 criterion at sites-1 to -4 in Table 1 while employing (**a**) the MA-based technique with a 10-min window, (**b**) the RR-based technique with a limit of 5% of the nominal rating per minute.

Table 4. The Pearson correlation coefficient between the determined SBOC and the SIVI for the considered sites in Table 1.

Site	MA (10 min)	RR Limit (5%)
1	0.7786	0.5633
2	0.7348	0.5750
3	0.8577	0.5966
4	0.8180	0.6981
5	0.7724	0.6914
6	0.7755	0.5629
7	0.7302	0.4431
8	0.8294	0.6383
9	0.7521	0.4469
10	0.7849	0.4334
11	0.8149	0.4621
Average of all sites	0.7862	0.5556

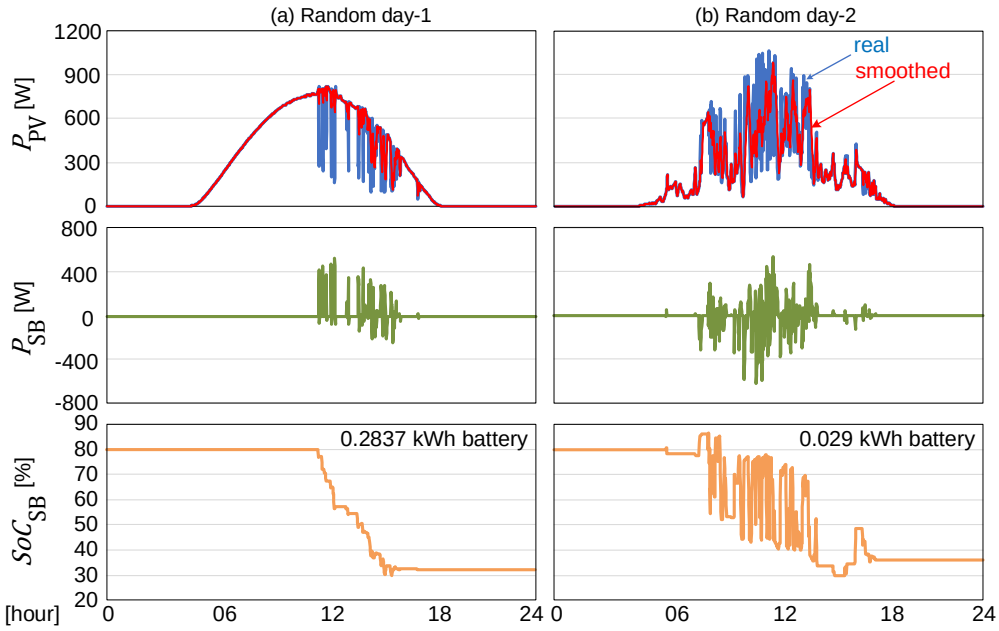

Figure 7. Performance of the microgrid in Figure 1 when using an SB, defined under the RR technique with 10% limit at site-5 on two random days of (**a**) 20 November 2017, (**b**) 18 December 2017.

The difference between the two days is the number of upward and downward ramps. The day with a relatively low SIVI has mainly downward ramps, thus requiring the SB to discharge for most of the day. On the other hand, the day with a high SIVI has a more symmetrical distribution of upward and downward ramps, allowing the SB to charge and discharge throughout the day. Therefore, for the RR technique, the direction of ramping events is a key factor for sizing the SB. The SIVI provides a crude proxy for the amount of ramping that will be observed as a day with a high SIVI is more likely to exhibit asymmetrical ramping events requiring higher SBOC. However, the outliers in these two figures show that this is not always true.

Figure 8 demonstrates the SBOC selected for P95 PONE at the 11 study sites in Table 1, using the MA- and RR-based techniques. This figure illustrates the results using the chronological simulation method, while Table 5 lists the results from the chronological simulation method, as well as the proposed approximate method, using the linear regression and the observed SIVI and their difference. The results support the previous observation that the MA is strongly correlated with the SIVI. The approximate method is inherently conservative because it adds the standard error to the linear regression, and the results in Table 5 show a fairly consistent positive deviation of within 7 to 25%. On the other hand, the large positive and negative deviations found in the results for the RR technique indicate that the approximate method does not accurately predict the SBOC.

Figure 9a,b show the linear regression using the MA and RR techniques and with the data from all of the sites used in the study in Figure 8. The regression coefficients for the MA and RR algorithms, used in (8), are provided in Table 6. It is to be noted that these coefficients are based on the model parameters used in this study (i.e., the SB's type, chemistry and DoD, the PV parameters, etc.) and may not be accurate if these parameters are changed.

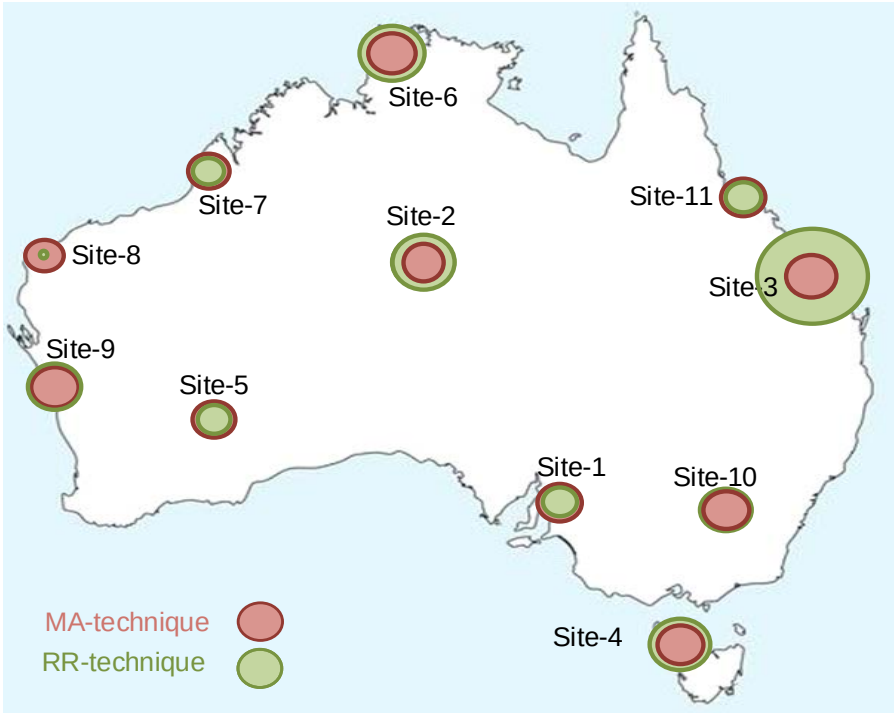

Figure 8. Comparison of the chronological simulation-based determined SBOC using a 10-min MA and 5% RR techniques for the 11 study sites considered in Table 1.

Table 5. Comparison of the determined SBOC by the detailed and proposed approximate models and their difference, using the P95 desired level for all considered sites in Table 1 under the 10-min MA and 5% RR techniques.

Site No.	**MA (10-min)**			**RR Limit (5%)**		
Model	**Detailed [kWh/kWp]**	**Approximate [kWh/kWp]**	**Deviation [%]**	**Detailed [kWh/kWp]**	**Approximate [kWh/kWp]**	**Deviation [%]**
1	0.140	0.150	7.1	0.111	0.149	34.2
2	0.142	0.152	7.0	0.212	0.152	−28.3
3	0.159	0.175	10.1	0.362	0.188	−48.1
4	0.144	0.179	24.3	0.198	0.194	−2.0
5	0.136	0.163	19.9	0.109	0.168	54.1
6	0.150	0.167	11.3	0.214	0.176	−17.8
7	0.130	0.152	16.9	0.100	0.151	51.0
8	0.123	0.140	13.8	0.019	0.132	594.7
9	0.151	0.177	17.2	0.174	0.192	10.3
10	0.144	0.165	14.6	0.166	0.173	4.2
11	0.140	0.154	10.0	0.118	0.155	31.4

Table 6. Coefficients for the suggested approximate method used in the SBOC's calculation.

Technique	α	β	σ
MA with 10-min window	0.0046	0.0567	0.0315
RR with 5% ramp limit	0.0074	−0.0221	0.0709

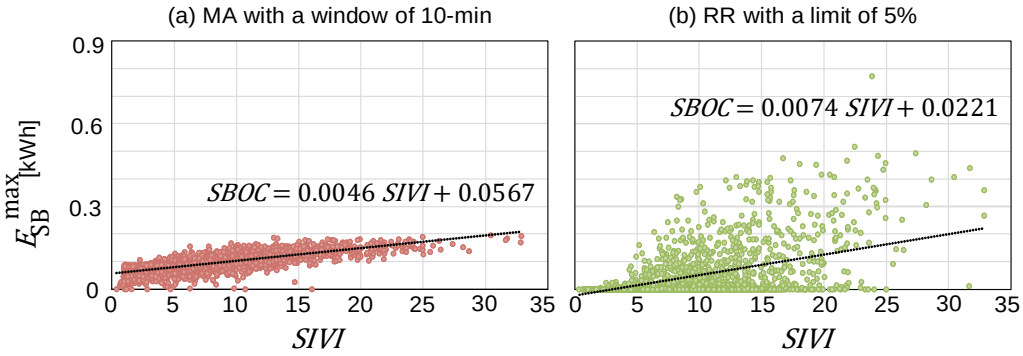

Figure 9. Linear regression results for all sites using (**a**) MA-based technique with a 10-min window and (**b**) RR-based technique with a limit of 5% of the nominal rating per minute.

5. Comparative Analysis

To illustrate the superior performance of the proposed technique versus the existing similar techniques, the detailed model described in this paper is compared against two SBOC sizing approaches that are commonly found in the literature.

The first method is the peak energy exchange method [18–20]. In this method, the energy exchanged between the SB and the microgrid is integrated over an entire day (allowing for recharging at night), and the maximum value denotes the peak energy exchange for the day.

This process is repeated for each day of the year, and the maximum value of the year is selected as the SBOC. The second common method is the hourly chronological simulation method [13,14]. This method is structurally similar to the method described in Appendix A, with the key differences being that the sampling resolution is hourly, and the SB is sized to have sufficient capacity for the entire year (i.e., there is no nightly recharging).

The above SB sizing methods are implemented for site-1 using the MA technique with a 10-min window. To facilitate a fair comparison between the methods, a maximum allowed DoD of 70% and initial SoC of 80% are applied and nightly recharging is assumed. The results of the comparison are presented in Table 7, showing the SBOC and the implied coverage over the full year, i.e., a coverage of 95% means that the SB is sufficiently sized for 95% of the year (347 days). The proposed methods (both detailed and approximate) yield similar SBOC values to the peak energy exchange method, although the SBOC from the peak energy exchange method has lower coverage as this method does not consider the SB's efficiencies or charge/discharge characteristics. Note also that the coverage in the proposed methods is a selected desired value and can be modified based on the SB's design criteria. As expected, the hourly chronological simulation method yields a significantly larger SBOC than the other methods due to the effect of the course of 1-h sampling resolution filtering out short-term variations in solar irradiance.

The study in Figure 9a illustrates that the SB sizing under the MA control technique is quite highly correlated to the SIVI of the site. As a result, when determining the SBOC for a specific location, the system planner or designer does not need the high-resolution irradiance data for the particular site location, but can use an estimate of the SIVI or the SIVI measured at a nearby location. This is because, in principle, the linear regression equation of (8) is applicable to any arbitrary site, provided that an estimate of the SIVI is known. This is the key practical use of the proposed approximate method.

Table 7. Comparison of SBOC sizing methods for site-1 using the MA-based technique with a 10-min window.

SBOC Sizing Method		SBOC [kWh/kWp]	Annual Coverage [%]
Existing Methods	Peak energy exchange	0.131	92.8
	Hourly chronological simulation	0.619	100.0
Methods of this paper	1-min chronological simulation (P95 desired level)	0.140	95.0
	Approximate method (P95 desired level)	0.150	96.5

6. Sensitivity Analysis

Sensitivity analysis was carried out to evaluate the variations in the determined SBOC against the key assumptions in the studies; i.e., the window size of the MA technique, the limit of the RR technique, as well as the SB's maximum allowed DoD and the desired initial SoC. The results of these studies are presented in Figure 10a–d, while in each of the sensitivity analyses, all other key parameters are assumed to be fixed as per Section 4.1.

Figure 10. The sensitivity of the determined SBOC to the (**a**) window size of the MA technique for a window of 5 to 20 min, (**b**) the limit of the RR technique for a limit of 1 to 15%, (**c**) a maximum allowed DoD of 80 to 50% for the SB, (**d**) a desired initial SoC of 60 to 90% for the SB, versus the observed $SIVI$.

6.1. Window Size of the MA Technique

As seen in Figure 10a, as expected, the SBOC increases as the MA window size is expanded from 5 to 20 min, with roughly a threefold increase. There is also an increase in the dispersion of the SBOC as the window size is expanded, with $\sigma = 0.0191$ for a 5-min window and $\sigma = 0.0494$ for a 20-min window.

6.2. Limit of the RR Technique

As shown in Figure 10b, the SBOC increases as the ramp rate limit decreases from 15 to 1% of the nominal rating per minute. As an example, an average SBOC of 0.0024 kWh/kWp is observed for a 15% ramp rate limit, while an average SBOC of 0.0615 kWh/kWp is seen for a 1% ramp rate limit. Similar to the window size of the MA technique, there is an increase in the dispersion of the SBOC as the limit of the RR technique is tightened, with $\sigma = 0.0102$ for a 15% limit and $\sigma = 0.1311$ for a 1% limit.

6.3. SB's Maximum Allowed DoD

The maximum allowed DoD may be a material parameter during the design process as not only does the maximum allowed DoD affect the battery life, but different battery technologies also have different maximum DoDs. As an example, [37] reported this parameter as varying between 53 and 100% depending on the battery technology. As illustrated in Figure 10c, the SBOC increases as its maximum allowed DoD decreases from 80 to 50%. At an allowed DoD of 80%, the mean SBOC is 0.0564 kWh/kWp, while it increases to 0.1254 kWh/kWp for a DoD of 50%.

6.4. SB's Initial SoC

As seen in Figure 10d, the SBOC increases as the SB's expected initial SoC decreases from 90 to 60%; however, the impacts are relatively small. For example, the mean SBOC is 0.0822 kWh/kWp for an initial SoC of 90%, which slightly increases to 0.0949 kWh/kWp for an initial SoC of 60%. As such, through the above sensitivity analyses, it can be seen that the SBOC is largely invariant to the initial SoC, and a value of 70–80% is suggested to provide sufficient headroom for the SB's charging and discharging. The sensitivity analyses also show that the maximum allowed DoD has a moderate impact on the SBOC, and it is recommended that it is set above 60%, although cycle-life considerations should also be taken into account.

The sensitivity analyses also showed that the RR becomes less correlated with the SIVI as the ramp rate limit increases, e.g., r = 0.5927 for a ramp rate limit of 1%, and r = 0.43587 for a ramp rate limit of 15%. This is because a day with a high SIVI can have many small fluctuations that do not exceed the ramp rate limit; thus, the SB does not need to be called into action.

7. Practical Considerations and Limitations

This study uses solar irradiance data with a 1-min resolution to capture the short-term temporal SIVI in the output power of the PV system. A question that arises is whether a 1-min resolution adequately covers the range of temporal fluctuations in the solar irradiance. For example, [38] reports variations of above 50% in 1 s for a 48 kWp PV system. However, the empirical probability of such variations was found to be 0.000235% (or roughly 2 h in a year). Ref. [38] also reports that variations of less than 10% in 1 s represent 99.86% of all observations. For 1-min resolutions, variations of less than 10% represent 95.11% of all observations. Based on these findings, it is proposed that 1-min resolution data be considered as the minimum resolution, while below 1-min resolutions may be used for higher coverage.

It is worth noting that the Bureau of Meteorology's weather stations are single measurement points, and any natural smoothing effects due to spatial diversity [29] are ignored in this study. For small centralized microgrid systems, the absence of spatial smoothing is un-

likely to significantly impact the results; however, ignoring the spatial smoothing for larger PV systems or distributed systems will lead to more conservative (less optimal) results.

It is to be noted that differences in the weather from one year to another may result in a calculated SBOC that is not truly optimal for future conditions. However, as the SBOC is essentially a capital investment prediction, it needs to be based on historical data. This paper suggests that at least one year of historical data are required to adequately cover the seasonal variations. However, it may be more prudent to use multi-year data to capture longer-term (inter-year) variations, such as natural climate cycles, e.g., El Niño and La Niña events. However, in practice, this may be contingent on the availability and/or project economics of collecting longer-term data.

8. Conclusions

This paper has focused on deriving a correlation between the SBOC and the SIVI based on the two most commonly used techniques of MA and RR. The studies were based on a large solar irradiance dataset with a 1-min resolution for a full calendar year across 11 locations. The studies show that the determined SBOC under the MA technique is quite strongly correlated with the daily SIVI, and this observation can be used to develop relatively accurate empirical estimates for the SBOC, which is solely based on the SIVI. A comparison with other SBOC sizing methods indicates that the proposed method is comparable to the peak energy exchange method but has greater flexibility as the level of coverage is an input variable for the SB's sizing algorithm. The sensitivity analyses also show that the SB's initial SoC does not significantly influence the SBOC and maximum allowed DoD. The results of this study also indicate that the SBOC determined using the RR technique is weakly correlated with the SIVI, and as a result, the approximate empirical method using the RR technique-based linear regressions has limited accuracy. As a result, a future research direction can be focused on identifying a more appropriate metric than the SIVI to quantify the solar irradiance variabilities when using the RR technique.

Author Contributions: Conceptualization, J.S. and F.S.; methodology, J.S.; validation, J.S.; writing—original draft preparation, J.S.; writing—review and editing, J.S. and F.S.; supervision, F.S. All authors have read and agreed to the published version of the manuscript.

Funding: This research received no external funding.

Data Availability Statement: Data are unavailable due to privacy restrictions.

Conflicts of Interest: The authors declare no conflict of interest.

Nomenclature

1. Abbreviations

CDF	Cumulative distribution function
DoD	Depth of discharge
GHI	Global horizontal irradiance
MA	Moving average
PONE	Probability of non-exceedance
PV	Photovoltaic
RR	Ramp rate
SB	Smoothing battery
SBOC	Smoothing battery's optimal capacity
SIVI	Solar irradiance variability index
SoC	State of charge

2. Parameters and Variables

E_{SB}^{nom}	SB's nominal capacity
$\left(E_{SB}^{nom}\right)^{pred}$	SB's nominal capacity defined by linear regression
k_{RRL}	RR limit

N_w	MA window size
P_{MA}	Smoothed output using MA technique
P_{PV}	Raw (unsmoothed) output from PV system
P_{RR}	Smoothed output using RR control technique
P_{SB}^{MA}	SB's net output under the MA control technique
P_{SB}^{RR}	SB's net output under the RR control technique
$SBOC^{ap}$	Approximate SBOC
ΔP_{max}	Maximum allowable change in PV output in a time step (based on RR control limit)
ΔT	Averaging interval for SIVI calculation

Appendix A. Chronological Simulation Method

The chronological simulation method used in this paper is a numerical solution to the SBOC selection problem in (7). The method works by first optimizing the SB for each day and then aggregating the results to select the SBOC.

Note that it is assumed that the SB is recharged (or discharged) each night to maintain a fixed (desired) initial SoC in the morning (e.g., 80%). This assumption is in line with [18,19]. This is because the SB capacity can be minimized by not having to consider the end-of-day SoC. In fact, the studies of this paper find that it is rare for the end-of-day SoC to be higher than the initial SoC because: (a) a preponderance of upward PV output ramps throughout the day; (b) an SB needs to be recharged at some point (e.g., every night or every week or every month).

Appendix A.1. SB Section for a Single-Day

The chronological simulation is executed for every simulation day at 1-min time steps (i.e., 1440 time steps per 24-h simulation) to capture the variations in the demand and output power of the PV system. At each time step, the computation steps are as below:

(a) Retrieving the solar irradiance for the time step from the available dataset;
(b) Calculating the PV system's expected output power from (A1) in Appendix B;
(c) Employing the MA- or RR-based smoothing technique and calculating the SB's charging/discharging status and level from (5) or (6);
(d) Calculating the smoothed output power of the PV system considering the SB's influence;
(e) Updating the SB's SoC from the Kinetic battery model described in (A2) and (A3) in Appendix B;
(f) Applying the SB's empty or full status (based on $SoC_{\mathrm{SB}}(t)$) to update its charging/discharging level, if required.

For each simulation day, the problem of (7) is solved using a binary search algorithm [39], where the SB's capacity is adjusted up and down at each iteration depending on whether the SoC constraints are met. The binary search algorithm ends when the difference between two successive iterations is below a nominated error tolerance level. Figure A1 illustrates the flowchart of this process.

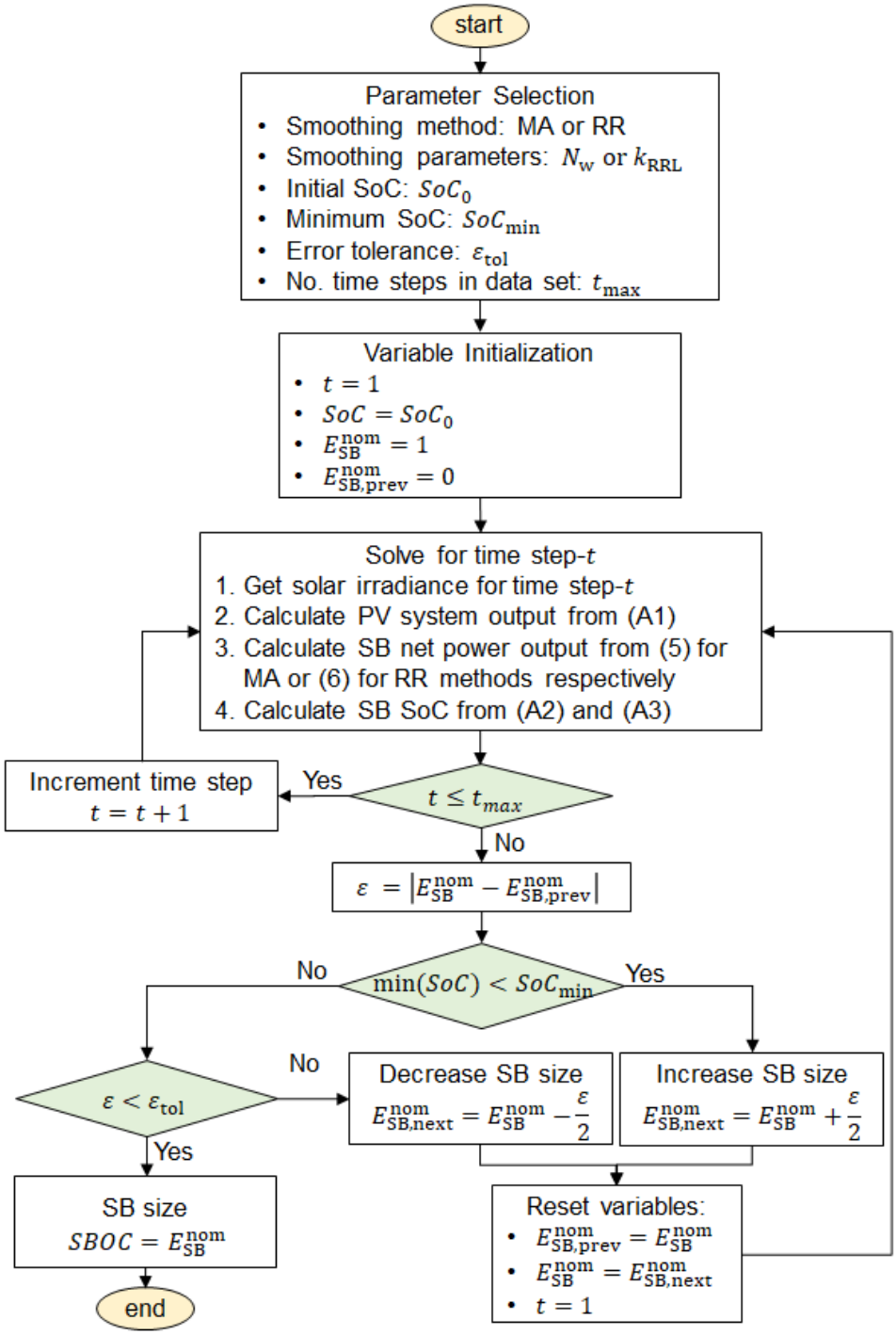

Figure A1. Flowchart of the algorithm selecting the SB for a single-day.

Appendix A.2. SBOC Selection

It was demonstrated in Section 5 that the results of the studies for both the MA- and RR-based smoothing techniques typically show several days in the year that can be marked as outliers in terms of the SBOC and/or the SIVI. Therefore, from an economic standpoint, there are diminishing investment returns from an SB that covers 100% of all cases (i.e., P100). As such, it is more prudent to select a smoothing level that covers the majority (e.g., 90 or 95%) of the cases (i.e., P90 and P95) and allows the curtailment of the PV system for the rest of the time. As such, the SBOC selection is based on the distribution of the

single-day SB selection results using a pre-selected (desired) smoothing level (e.g., P90 or P95).

The steps for selecting the SBOC are as follows:

(a) Collecting 1-min (or higher) resolution solar irradiance data for the site over at least one year;
(b) Running the single-day SB selection for each day in the dataset;
(c) Calculating the empirical CDFs and PONE levels for the dataset;
(d) Selecting a smoothing level based on the PONE of the results and calculating the SBOC according to selected smoothing level.

Appendix B. Modeling of PV and SB Systems

The output power of the PV system at the coupling point of the inverter at each time step of $t\left(P_{\mathrm{pv}}(t)\right)$ can be calculated using the simplified model of [40]:

$$P_{\mathrm{pv}}(t) = GHI(t) \times P_{\mathrm{nom}} \times k_{\mathrm{e}} \times k_{\mathrm{m}} \times \left(1 - k_{\mathrm{pt}} \times T_{\mathrm{amb}}(t)\right) \times \eta_{\mathrm{inv}} \tag{A1}$$

where k_{e} is the environmental derating factor to account for soiling, dust, etc. [%], k_{m} is the manufacturer tolerance derating factor [%], k_{pt} is the power-temperature coefficient [%/°C], $T_{\mathrm{amb}}(t)$ is the ambient temperature at time step t [°C], and η_{inv} is the inverter's efficiency [%]. It is to be noted that this simplified model does not consider the effects of the PV array's tilt angle and azimuth nor the albedo (ground reflectance). The inverter is also assumed to be fully rated to the peak output power of the PV array and no oversupply coefficient is considered (i.e., dc:ac ratio is 1).

The Kinetic battery model developed in [41–43] is used in the simulation model to calculate the amount of energy that can be transferred to and from the SB at each time step. The model reflects the observation that a battery's capacity tends to decrease with an increasing rate of charge or discharge (rate capacity effect). The Kinetic battery model was selected as it can adequately capture non-linear recovery and rate capacity effects across different battery technologies [22] and thus has been widely used in similar software tools such as HOMER. The total charge in a battery is divided into an "available" charge (q_1 [Ah]), which is energy that is accessible for immediate use, and a "bound" charge (q_2 [Ah]), which is energy that is chemically bound, but can be released at a certain rate. The flows of available and bound charges can be described as:

$$\begin{array}{c} \frac{dq_1}{dt} = -(I + k_1(1-k_2)q_1 - k_1k_2q_2) \\ \frac{dq_2}{dt} = k_1(1-k_2)q_1 - k_1k_2q_2 \end{array} \tag{A2}$$

where I is the charge or discharge current [A], k_1 is a rate constant at which chemically bound charge becomes available and k_2 is the ratio of available charge to total capacity. The differential equations can be solved for each time step t using Laplace transforms as:

$$\begin{array}{c} q_1 = q_{1,0}e^{-k_1\Delta t} + \frac{(q_0k_1k_2 - I)\left(1-e^{-k_1\Delta t}\right)}{k_1} - \frac{Ik_2\left(k_1\Delta t - 1 + e^{-k_1\Delta t}\right)}{k_1} \\ q_2 = q_{2,0}e^{-k_1\Delta t} + q_0(1-k_2)\left(1-e^{-k_1\Delta t}\right) - \frac{I(1-k_2)\left(k_1\Delta t - 1 + e^{-k_1\Delta t}\right)}{k_1} \end{array} \tag{A3}$$

where $q_{1,0}$, $q_{2,0}$, and q_0 are the available, bound, and total charges at the beginning of the time step and Δt is the length of the time step (1 min = 1/60 h).

It is to be noted that k_1 and k_2 are specific to a battery's charging and/or discharging performance, which in turn varies with battery chemistry, capacity and construction. The constants can be estimated using a non-linear least squares algorithm that fits the battery constants with actual charge/discharge performance characteristics, e.g., from a battery manufacturer's datasheet. Also, in the studies of this paper, the flow of charge into and out of the battery is also reduced by the conversion losses from the battery's bi-directional converter. Note that the kinetic battery model does not consider the effects of temperature, self-discharge, and cycle degradation/ageing on the capacity and SoC.

Appendix C. Technical Parameters

The employed parameters in the modeled PV and battery in Appendix A are retrieved from [35,36,44,45], as given in Tables A1 and A2.

Table A1. Considered PV parameters in the simulations.

Parameter	Symbol	Value	Remarks
PV nominal rating	P_{nom}	1000 [Wp]	
Environmental derating factor	k_e	90 [%]	Assuming light to moderate soiling and dust
Manufacturer output tolerance	k_m	95 [%]	AS/NZS 4509.2 Recommendation [40]
Power-temperature coefficient	k_{pt}	0.38 [%]	Datasheet value for a crystalline silicon module from a Tier-1 manufacturer [44]
Inverter efficiency	η_{inv}	95 [%]	Average value for a grid-tied PV inverter from a Tier-1 manufacturer [45]

Table A2. SB's discharge characteristics [43].

Discharge time (hours)	1	3	5	8	10
Discharge current (A)	242.4	115.7	79.8	55.23	47.01

References

1. Nayar, C. Innovative remote micro-grid systems. *Int. J. Environ. Sustain.* **2012**, *1*, 53–65. [CrossRef]
2. *Lazard's Levelized Cost of Energy Analysis*, Version 11.0; 2017; pp. 1–21. Available online: https://www.philipwarburg.com/wp-content/uploads/attachments/lazard-levelized-cost-of-energy-version-110.pdf (accessed on 1 July 2023).
3. Susanto, J.; Shahnia, F.; Ludwig, D. A framework to technically evaluate integration of utility-scale photovoltaic plants to weak distribution systems. *Appl. Energy* **2018**, *231*, 207–221. [CrossRef]
4. Somayajula, D.; Crow, M.L. An integrated active power filter-ultracapacitor design to provide intermittency smoothing and reactive power support to the distribution grid. *IEEE Trans. Sustain. Energy* **2014**, *5*, 1116–1125. [CrossRef]
5. Wang, G.; Ciobotaru, M.; Agelidis, V.G. Power smoothing of large solar PV plant using hybrid energy storage. *IEEE Trans. Sustain. Energy* **2014**, *5*, 834–842. [CrossRef]
6. Teleke, S.; Baran, M.E.; Bhattacharya, S.; Huang, A.Q. Rule-based control of battery energy storage for dispatching intermittent renewable sources. *IEEE Trans. Sustain. Energy* **2010**, *1*, 117–124. [CrossRef]
7. Datta, M.; Senjyu, T.; Yona, A.; Funabashi, T. Photovoltaic output power fluctuations smoothing by selecting optimal capacity of battery for a photovoltaic-diesel hybrid system. *Electr. Power Compon. Syst.* **2011**, *39*, 621–644. [CrossRef]
8. Wang, D.; Ge, S.; Jia, H.; Wang, C.; Zhou, Y.; Lu, N.; Kong, X. A demand response and battery storage coordination algorithm for providing microgrid tie-line smoothing services. *IEEE Trans. Sustain. Energy* **2014**, *5*, 476–486. [CrossRef]
9. Khodabakhsh, R.; Sirouspour, S. Optimal control of energy storage in a microgrid by minimizing conditional value-at-risk. *IEEE Trans. Sustain. Energy* **2016**, *7*, 1264–1273. [CrossRef]
10. Sun, Z.; Li, Z.; Gao, L.; Zhao, X.; Han, D.; Gan, S.; Guo, S.; Niu, L. Grafting Benzenediazonium Tetrafluoroborate onto LiNixCoyMnzO2 materials achieves subzero-temperature high-capacity lithium-ion storage via a diazonium soft-chemistry method. *Adv. Energy Mater.* **2018**, *9*, 1802946. [CrossRef]
11. Sun, Z.; Li, Z.; Wu, X.L.; Zou, M.; Wang, D.; Gu, Z.; Xu, J.; Fan, Y.; Gan, S.; Han, D.; et al. A practical li-ion full cell with a high-capacity cathode and electrochemically exfoliated graphene anode: Superior electrochemical and low-temperature performance. *ACS Appl. Energy Mater.* **2019**, *2*, 486–492.
12. Sun, Z.; Wu, X.L.; Xu, J.; Qu, D.; Zhao, B.; Gu, Z.; Li, W.; Liang, H.; Gao, L.; Fan, Y.; et al. Construction of bimetallic selenides encapsulated in nitrogen/sulfur co-doped hollow carbon nanospheres for high-performance sodium/potassium-ion half/full batteries. *Nano Micro. Small* **2020**, *16*, 1907670. [CrossRef]
13. Senjyu, T.; Datta, M.; Yona, A.; Funabashi, T.; Kim, C.H. PV output power fluctuations smoothing and optimum capacity of energy storage system for PV power generator. *Int. Conf. Renew. Energy Power Qual. (ICREPQ)* **2018**, *1*, 35–39. [CrossRef]
14. Marcos, J.; Storkël, O.; Marroyo, L.; Garcia, M.; Lorenzo, E. Storage requirements for PV power ramp-rate control. *Sol. Energy* **2014**, *99*, 28–35. [CrossRef]
15. Marcos, J.; de la Parra, I.; Garcia, M.; Marroyo, L. Control strategies to smooth short-term power fluctuations in large photovoltaic plants using battery storage systems. *Energies* **2014**, *7*, 6593–6619. [CrossRef]
16. Sandhu, K.; Mahesh, A. A new approach of sizing battery energy storage system for smoothing the power fluctuations of a PV/wind hybrid system. *Int. J. Energy Res.* **2016**, *40*, 1221–1234. [CrossRef]
17. Mahesh, A.; Sandhu, K.; Rao, K.V. Optimal sizing of battery energy storage system for smoothing power fluctuations of a PV/wind hybrid system. *Int. J. Emerg. Power Syst.* **2017**, *18*, 20160105. [CrossRef]

18. Sasmal, R.P.; Sen, S.; Chakraborty, A. Solar photovoltaic output smoothing: Using battery energy storage system. In Proceedings of the National Power System Conference, Bhubaneswar, India, 19–21 December 2016; pp. 1–5.
19. Desta, A.; Courbin, P.; Sciandra, V. Gaussian-based smoothing of wind and solar power productions using batteries. *Int. J. Mech. Eng. Robot. Res.* **2017**, *6*, 154–159. [CrossRef]
20. Nazaripouya, H.; Chu, C.C.; Pota, H.R.; Dagh, R. Battery energy storage system control for intermittency smoothing using optimized two-stage filter. *IEEE Trans. Sustain. Energy* **2018**, *9*, 664–675. [CrossRef]
21. Li, X.; Hui, D.; Lai, X. Battery energy storage station-based smoothing control of photovoltaic and wind power generation fluctuations. *IEEE Trans. Sustain. Energy* **2013**, *4*, 464–473. [CrossRef]
22. Meng, J.; Luo, G.; Ricco, M.; Swierczynski, M.; Stroe, D.I.; Teodorescu, R. Overview of Lithium-ion battery modeling methods for state-of-charge estimation. *Appl. Sci.* **2018**, *8*, 659. [CrossRef]
23. Song, M.; Gao, C.; Shahidehpour, M.; Li, Z.; Lu, S.; Lin, G. Multi-time-scale modeling and parameter estimation of TCLs for smoothing out wind power generation variability. *IEEE Trans. Sustain. Energy* **2019**, *10*, 105–118. [CrossRef]
24. Zhang, F.; Wang, G.; Meng, K.; Zhao, J.; Xu, Z.; Dong, Z.Y.; Liang, J. Improved cycle control and sizing scheme for wind energy storage system based on multiobjective optimization. *IEEE Trans. Sustain. Energy* **2017**, *8*, 966–977. [CrossRef]
25. Zhou, Y.; Yan, Z.; Li, N. A novel state of charge feedback strategy in wind power smoothing based on short-term forecast and scenario analysis. *IEEE Trans. Sustain. Energy* **2017**, *8*, 870–879. [CrossRef]
26. Zhang, F.; Meng, K.; Xu, Z.; Dong, Z.; Zhang, L.; Wan, C.; Liang, J. Battery ESS planning for wind smoothing via variable-interval reference modulation and self-adaptive SOC control strategy. *IEEE Trans. Sustain. Energy* **2017**, *8*, 695–707. [CrossRef]
27. Savkin, A.V.; Khalid, M.; Agelidis, V.G. A constrained monotonic charging/discharging strategy for optimal capacity of battery energy storage supporting wind farms. *IEEE Trans. Sustain. Energy* **2016**, *7*, 1224–1231. [CrossRef]
28. Brekken, T.K.; Yokochi, A.; Von Jouanne, A.; Yen, Z.Z.; Hapke, H.M.; Halamay, D.A. Optimal energy storage sizing and control for wind power applications. *IEEE Trans. Sustain. Energy* **2011**, *2*, 69–77. [CrossRef]
29. Lohmann, G.M. Irradiance variability quantification and small-scale averaging in space and time: A short review. *Atmosphere* **2018**, *9*, 264. [CrossRef]
30. Australian Government Bureau of Meteorology—One Minute Solar Data. Available online: http://reg.bom.gov.au/climate/reg/oneminsolar (accessed on 1 October 2018).
31. Stein, J.S.; Hansen, C.W.; Reno, M.J. The variability index: A new and novel metric for quantifying irradiance and PV output variability. In Proceedings of the World Renewable Energy Forum, Denver, CO, USA, 13–17 May 2012; pp. 13–17.
32. Australian Renewable Energy Agency. Hybrid power generation for Australian off-grid mines. *Tech. Rep.* **2018**.
33. Ellis, A.; Schoenwald, D.; Hawkings, D.; Willard, S. PV output smoothing with energy storage. In Proceedings of the 38th IEEE Photovoltaic Specialists Conference, Austin, TX, USA, 3–8 June 2012; pp. 1523–1528.
34. Greenwood, W.; Lavrova, O.; Mammoli, A.; Cheng, F.; Willard, S. Optimization of solar PV smoothing algorithms for reduced stress on a utility-scale battery energy storage system. In Proceedings of the Electrical Energy Storage Applications and Technologies Conference, San Diego, CA, USA, 21–23 October 2013; Sandia National Laboratories: Albuquerque, NM, USA, 2013.
35. Olympic Batteries DC2-500 Technical Data Sheet. Available online: https://www.olympicbatteries.com.au/wp-content/uploads/2020/09/Spec-Sheet-for-DC2-500-AusCell.pdf (accessed on 1 July 2023).
36. SMA Sunny Boy Storage 3.7/5.0/6.0 Technical Data Sheet. Available online: https://files.sma.de/downloads/SBSxx-10-DS-en-31.pdf (accessed on 1 July 2023).
37. Terlouw, T.; AlSkaif, T.; Bauer, C.; van Sark, W. Multi-objective optimization of energy arbitrage in community energy storage systems using different battery technologies. *Appl. Energy* **2019**, *239*, 356–372. [CrossRef]
38. Marcos, J.; Marroyo, L.; Lorenzo, E.; Alvira, D.; Izco, E. Power output fluctuations in large scale PV plants: One year observations with one second resolution and a derived analytic model. *Prog. Photovolt. Res. Appl.* **2011**, *19*, 218–227. [CrossRef]
39. Press, W.H.; Tuekolsky, S.A.; Vetterling, W.T.; Flannery, B.P. *Numerical Recipes in C: The Art of Scientific Computing*, 2nd ed.; Cambridge University Press: Cambridge, UK, 2002; pp. 397–401.
40. *AS/NZS 4509.2*; Stand-Alone Power Systems—Part 2: System Design Guidelines. Standards Australia: Sydney, Australia, 2010.
41. Manwell, J.F.; Rogers, A.; Hayman, G.; Avelar, C.T.; McGowan, J.G.; Abdulwahid, U.; Wu, K. *Hybrid2: A Hybrid System Simulation Model, Theory Manual*; Technical Report; National Renewable Energy Laboratory: Golden, CO, USA, 2006.
42. Manwell, J.F.; McGowan, J.G.; Abdulwahid, U.; Wu, K. Improvements to the Hybrid2 battery model. In Proceedings of the American Wind Energy Association Windpower 2005 Conference, Denver, CO, USA, 15–18 May 2005.
43. Manwell, J.F.; McGowan, J. Extension of the kinetic battery model for wind/hybrid power systems. In Proceedings of the 5th European Wind Energy Association Conference, Macedonia, Greece, 10–14 October 1994; pp. 284–289.
44. Sunpower 225 Solar Panel Technical Data Sheet. Available online: https://www.energymatters.com.au/images/sunpower/SPR-225_com.pdf (accessed on 1 July 2023).
45. SMA Tripower 5000TL–12000TL Technical Data Sheet. Available online: https://files.sma.de/downloads/STP12000TL-DEN1723-V10web.pdf (accessed on 1 July 2023).